A Wideband Space-Time Model for MIMO Mobile Fading Channels

Zoran Latinovic, Ali Abdi, and Yeheskel Bar-Ness

Center for Communication and Signal Processing Research, Dept. of Elec. and Comp. Eng.,
New Jersey Institute of Technology, University Heights, 323 King Blvd., Newark, NJ 07102
Email: {zl3, ali.abdi, barness}@njit.edu

***Abstract*- In this paper, the circular ring model is proposed to model the signal statistics of a wideband multiple-input multiple-output (MIMO) channel. Based on the proposed model, a new space-time-frequency cross-correlation function is derived for the MIMO channel, in a compact mathematical form. The cross-correlation function includes various parameters of interest such as the distance between the base station and the user, spacing among antenna elements, user's speed and direction, as well as the angle spread and delay spread. In addition, the time of arrival probability density function and power delay profile of the circular ring model are derived and compared with measured data. The proposed model and the associated wideband space-time cross-correlation provide a convenient unified framework for the simulation of frequency selective mobile MIMO fading channels and the design of proper space-time coding and signal processing techniques over such channels.**

I. INTRODUCTION

Multiple-input multiple-output (MIMO) wireless systems have multiple antennas at both receiver and transmitter. Under the condition of uncorrelated antenna elements and Rayleigh fading, capacity of the system can be increased linearly with the number of antennas. Most of the theoretical works in the past [1]-[3] assumed that kind of simplified channel model, but in practice some correlation among the antenna elements may exist that can reduce the channel capacity.

Moreover, most papers in the past have focused on frequency-flat fading channels, whereas frequency selective channels have received significant attention due to the high demand for high-speed communications [4] [5].

The geometric channel model with a ring of scatterers around the user has been extensively used for a narrowband channel [6], mostly due to its simplicity. In the sequel we show that this model is not applicable to wideband channels due to unrealistic probability density function (PDF) it provides for time of arrival (TOA). The main contribution of this paper is a new geometric model that also exhibits good match to different characteristics of wideband measured channel data such as TOA PDF and power delay spectrum (PDS), also known as power delay profile. In addition, the proposed model is used to derive a closed-from space-time-frequency (STF) cross-correlation function among the links of a frequency selective MIMO mobile fading channel with multi-element transmit and receive antennas. This is the wideband extension of the narrowband correlation model of [7].

The rest of this paper is organized as follows. The circular ring wideband geometric-stochastic model for MIMO channels is introduced in Section II, whereas the new STF cross-correlation is derived in Section III. Section IV is devoted to the derivation of TOA PDF and PDS for the circular ring model. Comparison of the model with published wideband measurements, in terms of the TOA PDF and PDS is the topic of Section V. Concluding remarks are given in Section VI.

II. THE CIRCULAR RING WIDEBAND MIMO MODEL

Consider the multi-element antenna system configuration, shown in Fig. 1, where the base station (BS) and the user have n_{BS} and n_U omni-directional antenna elements in the horizontal plane, respectively. Without loss of generality, the case of $n_{BS} = n_U = 2$ (a 2×2 MIMO channel) has been considered. The convention for numbering the antenna elements is such that $1 \le l \le m \le n_U$ and $1 \le p \le q \le n_{BS}$. The BS receives the signal through the narrow beamwidth 2Δ, while the user receives the signal from a large number of surrounding local scatterers, impinging the user from different directions. We assume that the waves are planar and bounced only once. The i^{th} scatterer is represented by S_i, R_i is the distance between the i^{th} scatterer and the user and D is the distance between the BS and the user. All scatterers are located on the circular ring, with the distance from the user within the range $R_1 \le R_i \le R_2$. Clearly, Δ, R_2, and D are related through $\tan(\Delta) = R_2/D$.

Let us consider the downlink with no transmit beamforming. Let $s_p(t)$ represent the complex envelope of the signal transmitted from the p^{th} BS array element and $r_l(t)$ the complex envelope of the signal received by the l^{th} user's array element. The complex lowpass equivalent time-variant channel response between BS_p and U_l is given by $h_{lp}(\tau,t)$. Based on the vector notations $\boldsymbol{s}(t) = [s_1(t)...s_{n_{BS}}(t)]^T$ and $\boldsymbol{r}(t) = [r_1(t)...r_{n_U}(t)]^T$, with $(\cdot)^T$ as the transpose operator, the complex lowpass equivalent input-output equation for the frequency selective MIMO fading channel can be written as

$$\boldsymbol{r}(t) = \boldsymbol{H}(\tau,t) * \boldsymbol{s}(t) + \boldsymbol{n}(t), \tag{1}$$

where $\boldsymbol{H}(\tau,t)$ is the $n_U \times n_{BS}$ matrix, where the entries are the input delay-spread functions, defined by Bello [8], such that $[\boldsymbol{H}(\tau,t)]_{lp} = h_{lp}(\tau,t)$, $*$ denotes convolution and $\boldsymbol{n}(t)$ stands for the complex envelope of the additive white Gaussian noise (AWGN) with zero mean vector and the diagonal covariance matrix, i.e., $E[\boldsymbol{n}(t)\boldsymbol{n}^H(t)] = P_{noise}\boldsymbol{I}_{n_U}$, where P_{noise} is the noise power at each receiver, $\boldsymbol{I}_{n_U}$ is the $n_U \times n_U$ identity matrix, and $(\cdot)^H$ denotes Hermitian transposition. The dependence of $\boldsymbol{H}(\tau,t)$ on the delay τ is a result of channel frequency selectivity (delay spread), whereas the dependence on time t is a result of user mobility (Doppler spread). Besides the frequency and time selectivity, we have also taken into account the effect of space selectivity through the realistic assumptions of non-isotropic scattering and non-uniform distribution of angle of arrival (AOA) [9]. The effect of antenna spacing at both the base station and the user is also included.

In the channel model depicted in Fig. 1, the local scatterers are assumed to be fixed, independent of time, and the motion of the user is characterized by its speed v and the direction of the motion γ. These assumptions are necessary for obtaining a stationary space-time-frequency correlation function. The same assumptions can be found, for example, in [6] and [10] for the temporal correlation model, and in [11] and [12] for the spatio-temporal correlation model. Clearly, depending on the user's speed, the STF correlation function derived in the next section will be accurate only over a time duration that is much smaller than R_1/v.

Let us define the power transferred through the $BS_p - U_l$ link as Ω_{lp}, where $\Omega_{lp} = E[|h_{lp}(t,\tau)|^2] \le 1$, under the assumption of the unit total transmit power. The plane waves emitted from the array element BS_p travel over paths with different lengths and after being scattered by the local scatterers around the mobile user, impinge the array element U_l from different directions. Since we consider the Rayleigh fading channel, no line of sight (LOS) component exists. Mathematical representation of this propagation mechanism, similar to that of [18], results in the following expression

$$h_{lp}(\tau,t) = \lim_{N\to\infty} \frac{1}{\sqrt{N}} \sum_{i=1}^{N} g_i \left(\zeta_i \cdot R_i\right)^{-n/2} \exp\{j\Psi_i - j2\pi\lambda^{-1}\left(\xi_{ip} + \xi_{li}\right) + j2\pi f_D t \cos(\phi_i^U - \gamma)\} \delta(\tau - \tau_i) \quad (2)$$

In the formula above, N is the number of independent scatterers S_i around the user, g_i represents the amplitude of the wave scattered by the i^{th} scatterer toward the user. ψ_i denotes the phase shift introduced by the i^{th} scatterer, ξ_{ip} and ξ_{li} are the distances shown in Fig. 1, which are functions of ϕ_i^U and R_i. Strictly speaking, the AOA depends on the antenna location at the user side. However, if the scatterers are located far from the user, i.e., $d_{lm} \ll R_1$ this dependence can be neglected and ϕ_i^U can be considered as the AOA for all the antenna elements. Similarly, the term $\xi_{ip} \cdot \xi_{li}$ related to the amplitude attenuation has been replaced with $\zeta_i \cdot R_i$. Note that, however, replacing $\xi_{ip}(\xi_{li})$ with $\zeta_i(R_i)$ in the exponent is inappropriate. Further, the wavelength is denoted by λ, $j^2 = -1$, $f_D = v/\lambda$ is the maximum Doppler shift, n represents the path loss exponent and finally τ_i is the travel time of the wave scattered by the i^{th} scatterer. Let assume that $\{g_i\}_{i=1}^{\infty}$ are independent and identically distributed (i.i.d) random variables with $E[g_i^2] = 1$, independent of $\{\psi_i\}_{i=1}^{\infty}$. It is reasonable to assume that $\{\psi_i\}_{i=1}^{\infty}$ are i.i.d. random variables with uniform distributions over $[0, 2\pi)$. One can easily show that $\Omega_{lp} = \lim_{N\to\infty} N^{-1} \sum_{i=1}^{N} E[g_i^2](\zeta_i \cdot R_i)^{-n}$. According to the statistical properties of the channel described above, central limit theorem implies that $h_{lp}(\tau,t)$ is a lowpass zero-mean complex Gaussian process. Hence, for each τ_i, the envelope $|h_{lp}(\tau_i,t)|$ is a Rayleigh process.

III. The New Space-Time-Frequency Cross-Correlation

The time-varying frequency response $T(f,t)$ is defined in [8] as the Fourier transform of $h(\tau,t)$, i.e., $T(f,t) = \Im_\tau\{h(\tau,t)\}$. For the wideband communication link $BS_p - U_l$ we have

$$T_{lp}(f,t) = \lim_{N\to\infty} \frac{1}{\sqrt{N}} \sum_{i=1}^{N} g_i \left(\zeta_i \cdot R_i\right)^{-n/2} \exp\{j\Psi_i - j2\pi\lambda^{-1}\left(\xi_{ip} + \xi_{li}\right) + j2\pi f_D t \cos(\phi_i^U - \gamma) - j2\pi f \tau_i\} \quad (3)$$

Now we define the normalized STF cross-correlation function between the time-varying frequency responses of two arbitrary communication links $T_{lp}(\tau,t)$ and $T_{mq}(\tau,t)$ as

$$\rho_{lp,mq}(\Delta f, \Delta t) = E[T_{lp}(f,t) T_{mq}^*(f+\Delta f, t+\Delta t)] \Big/ \sqrt{\Omega_{lp}\Omega_{mq}} \quad (4)$$

where $(\cdot)^*$ denotes the complex conjugate operation. According to the statistical properties of $\{g_i\}_{i=1}^{\infty}$ and $\{\psi_i\}_{i=1}^{\infty}$ discussed earlier and also Eq. (3), the cross-correlation function between $T_{lp}(\tau,t)$ and $T_{mq}(\tau,t)$ can be written as

$$\rho_{lp,mq}(\Delta f, \Delta t) = \Omega^{-1} \lim_{N\to\infty} \frac{1}{N} \sum_{i=1}^{N} E[g_i^2](\zeta_i \cdot R_i)^{-n} \times \exp\{-j2\pi\lambda^{-1}(\xi_{ip} - \xi_{iq} + \xi_{li} - \xi_{mi}) - j2\pi f_D \Delta t \cos(\phi_i^U - \gamma) + j2\pi \Delta f \tau_i\}. \quad (5)$$

where we are assuming $\Omega_{lp} = \Omega_{mq} = \Omega$. For large N, the contribution of the i^{th} scatterer, out of the total power Ω_{lp}, is proportional to $E[g_i^2](\zeta_i \cdot R_i)^{-n}/N$, which is equal to the infinitesimal power coming from the density of scatterers within $dRd\phi^U$ with the probability $f(\phi_i^U, R_i)$, i.e., $E[g_i^2](\zeta_i \cdot R_i)^{-n}/N = (\zeta(\phi_i^U, R_i) \cdot R_i)^{-n} f(\phi_i^U, R_i) dRd\phi^U$ (the reader may refer to [7] for the same type of argument for the narrowband case). Note that $f(\phi^U, R)$ is the joint PDF of ϕ^U and R. Now, Eq. (5) can be written as

$$\rho_{lp,mq}(\Delta f, \Delta t) = \Omega^{-1} \int_{R_1}^{R_2} \int_{-\pi}^{\pi} (\zeta(\phi^U, R) \cdot R)^{-n} \exp\{-j2\pi\lambda^{-1}(\xi_{\phi^U p} - \xi_{\phi^U q} + \xi_{l\phi^U} - \xi_{m\phi^U}) - j2\pi f_D \Delta t \cos(\phi^U - \gamma) + j2\pi c^{-1} \Delta f (\zeta_{\phi^U} + R)\} f(\phi^U, R) d\phi^U dR. \quad (6)$$

where $\xi_{\phi^U p}$ is the length of the path between the antenna element BS_p and the point on the ring of radius R, determined by ϕ^U, and so on.

Equation (6) gives the exact cross-correlation function which for a given $f(\phi^U, R)$, needs to be calculated numerically. In order to use some geometric properties, let us for a moment consider only scatterers that are located on a ring with the radius R. Then, the following relations can be derived using the law of cosines in appropriate triangles

$$\begin{aligned} \xi_{\phi^U p}^2 &= \delta_{pq}^2/4 + \zeta_{\phi^U}^2 - \delta_{pq}\zeta_{\phi^U}\cos(\alpha_{pq} - \phi_{\phi^U}^{BS}), \\ \xi_{\phi^U q}^2 &= \delta_{pq}^2/4 + \zeta_{\phi^U}^2 + \delta_{pq}\zeta_{\phi^U}\cos(\alpha_{pq} - \phi_{\phi^U}^{BS}), \\ \xi_{l\phi^U}^2 &= d_{lm}^2/4 + R^2 - d_{lm}R\cos(\phi^U - \beta_{lm}), \\ \xi_{m\phi^U}^2 &= d_{lm}^2/4 + R^2 + d_{lm}R\cos(\phi^U - \beta_{lm}), \end{aligned} \quad (7)$$

as well as the law of sines in the triangle $O_{BS}S_iO_U$

$$\sin(\phi^U - \phi_{\phi^U}^{BS}) D^{-1} = \sin(\phi_{\phi^U}^{BS}) R^{-1} = \sin(\phi^U)\zeta_{\phi^U}^{-1}. \quad (8)$$

The reasonable assumption of $D \gg R_2 > R_1 \gg \max(\delta_{pq}, d_{lm})$ for many practical cases of interest, which also implies that Δ is small, simplifies the equations drastically. This kind of assumption

is valid for a macrocells and some microcells. We use the approximate relations $\sqrt{1+\chi} \approx 1+\chi/2$, $\sin(\chi) \approx \chi$, and $\cos(\chi) \approx 1$, when χ is small. To begin with, the first equation in (8) yields $\phi_{\phi^U}^{BS} \approx \Delta \sin(\phi^U)$, as $\phi_{\phi^U}^{BS}$ and $\Delta \approx R/D$ are small. Consequently, equations in (7) can be written as

$$\begin{aligned}
\xi_{\phi^U p} &\approx \zeta_{\phi^U} - \delta_{pq}\left[\cos(\alpha_{pq}) + \Delta \sin(\alpha_{pq})\sin(\phi^U)\right]/2, \\
\xi_{\phi^U q} &\approx \zeta_{\phi^U} + \delta_{pq}\left[\cos(\alpha_{pq}) + \Delta \sin(\alpha_{pq})\sin(\phi^U)\right]/2, \\
\xi_{l\phi^U} &\approx R - d_{lm}\cos(\phi^U - \beta_{lm})/2, \\
\xi_{m\phi^U} &\approx R + d_{lm}\cos(\phi^U - \beta_{lm})/2, \\
\zeta_{\phi^U} &\approx D + R\cos(\phi^U).
\end{aligned} \tag{9}$$

Substitution of (9) into (6) yields the approximate cross-correlation function

$$\begin{aligned}
\rho_{lp,mq}(\Delta f, \Delta t) \approx \frac{1}{\Omega}\int_{R_1}^{R_2} (DR)^{-n} \exp\Big[& j2\pi\lambda^{-1}\delta_{pq}\cos(\alpha_{pq}) \\
& + j2\pi R c^{-1}\Delta f\left(1 + DR^{-1}\right)\Big] \int_{-\pi}^{\pi} \exp\Big\{ j2\pi\lambda^{-1}\Big[\delta_{pq}\Delta\sin(\alpha_{pq})\sin(\phi^U) \\
& + d_{lm}\cos(\phi^U - \beta_{lm})\Big] - j2\pi f_D \Delta t\cos(\phi^U - \gamma) \\
& + j2\pi R c^{-1}\Delta f\cos(\phi^U)\Big\} f(\phi^U) d\phi^U f(R) dR,
\end{aligned} \tag{10}$$

where c denotes the speed of light and we have assumed that ϕ^U and R are independent random variables, i.e., $f(\phi^U, R) = f(\phi^U) \cdot f(R)$. We further use the von Mises PDF for the AOA, as it fits very well the real data [13]

$$f(\phi^U) = \left(2\pi I_0(\kappa)\right)^{-1} \exp\left[\kappa\cos\left(\phi^U - \mu\right)\right], \quad \phi^U \in [-\pi, \pi), \tag{11}$$

where $I_0(.)$ is the zero[th] order modified Bessel function, $\mu \in [-\pi, \pi)$ accounts for the mean direction of AOA seen by the user, and $\kappa \geq 0$ controls the width of AOA.

After substitution of (11) into (10) and calculating the inner integral according to equation 3.338-4, p. 357 given in [14]

$$\int_{-\pi}^{\pi} \exp\left(x\sin z + y\cos z\right) dz = 2\pi I_0\left(\sqrt{x^2 + y^2}\right), \tag{12}$$

we obtain our key result in equation (13),

$$\begin{aligned}
\rho_{lp,mq}(\Delta f, \Delta t) \approx \frac{D^{-n}}{\Omega I_0(\kappa)} \int_{R_1}^{R_2} & \exp\left[jc_{pq}\cos(\alpha_{pq}) + je\left(1 + DR^{-1}\right)\right] \\
\times I_0 \Big(\Big\{ & \kappa^2 - a^2 - b_{lm}^2 - e^2 - c_{pq}^2\Delta^2\sin^2(\alpha_{pq}) + 2ab_{lm}\cos(\beta_{lm} - \gamma) \\
& + 2c_{pq}\Delta\sin(\alpha_{pq})\left[a\sin(\gamma) - b_{lm}\sin(\beta_{lm})\right] + 2ae\cos(\gamma) \\
& - 2b_{lm}e\cos(\beta_{lm}) - j2\kappa\left[a\cos(\mu - \gamma) - b_{lm}\cos(\mu - \beta_{lm})\right. \\
& \left. - c_{pq}\Delta\sin(\alpha_{pq})\sin(\mu) - e\cos(\mu)\right]\Big\}^{1/2}\Big) R^{-n} f(R) dR.
\end{aligned} \tag{13}$$

To simplify notation, we have defined $a = 2\pi f_D \Delta t$, $b_{lm} = 2\pi d_{lm}/\lambda$, $c_{pq} = 2\pi\delta_{pq}/\lambda$, and $e = 2\pi R\Delta f/c$. For a given $f(R)$, the cross-correlation function in (13) needs to be calculated, numerically.

IV. Time of Arrival PDF and Power Delay Spectrum

In order to validate our model, we compare the TOA PDF and PDS of the circular ring structure with measured data, in the next section. For this purpose, we need to consider the single-input single-output (SISO) version of the model, i.e., $d_{lm} = \delta_{pq} = 0$ and consequently $b_{lm} = c_{pq} = 0$. The cross-correlation function in (13) then simplifies significantly to

$$\begin{aligned}
\rho(\Delta f, \Delta t) \approx \frac{D^{-n}}{\Omega I_0(\kappa)} \int_{R_1}^{R_2} & \exp\left[je\left(1 + DR^{-1}\right)\right] \\
& \times I_0\Big(\Big\{\kappa^2 - a^2 - e^2 + 2ae\cos(\gamma) \\
& - j2\kappa\left[a\cos(\mu - \gamma) - e\cos(\mu)\right]\Big\}^{1/2}\Big) R^{-n} f(R) dR.
\end{aligned} \tag{14}$$

Before deriving the TOA PDF and PDS, recall that in Section I, it was mentioned that the TOA PDF of the ring model does not agree well with the decaying TOA PDF in typical outdoor channels [15]. Now we address this issue in detail. From the trigonometric relations in (9) and Fig. 1, the travel time of a plane wave originated from the BS, scattered from the scatterer located at R and ϕ^U, and received by the user, is given by

$$\begin{aligned}
\tau(\phi^U, R) &= c^{-1}\left(R + \sqrt{D^2 + R^2 + 2DR\cos\left(\phi^U\right)}\right) \\
&\approx c^{-1}\left(R + D + R\cos\left(\phi^U\right)\right),
\end{aligned} \tag{15}$$

Upon modeling the user AOA with the von Mises PDF in (11), transformation of the random variable ϕ^U using the second approximate equation of (15), which is valid for $D \gg R$, gives the following equation for the PDF of the relative TOA, for a particular radius R or, equivalently, the corresponding maximum relative delay $\tau_R^{\max} = 2R/c$

$$\begin{aligned}
f\left(\tau_r \middle| \tau_R^{\max}\right) \approx & \frac{\exp\left[\kappa\left(2\tau_r/\tau_R^{\max} - 1\right)\cos(\mu)\right]}{\pi\tau_R^{\max} I_0(\kappa)\sqrt{\left(1 - \tau_r/\tau_R^{\max}\right)\tau_r/\tau_R^{\max}}} \\
& \times\cosh\left[2\kappa\sqrt{\left(1 - \tau_r/\tau_R^{\max}\right)\tau_r/\tau_R^{\max}}\sin(\mu)\right],
\end{aligned} \tag{16}$$

where $\tau_r = \tau - \tau_{LOS}$ is the relative delay, i.e., $0 \leq \tau_r \leq \tau_R^{\max}$ and $\tau_{LOS} = D/c$. Furthermore, using the transformation $\tau_N = \tau_r/\tau_R^{\max}$ such that $0 \leq \tau_N \leq 1$, we can express the PDF of the normalized delay τ_N by

$$f(\tau_N) \approx \frac{\exp[\kappa(2\tau_N - 1)\cos(\mu)]}{\pi I_0(\kappa)\sqrt{\tau_N(1 - \tau_N)}}\cosh[2\kappa\sqrt{\tau_N(1 - \tau_N)}\sin(\mu)]. \tag{17}$$

Note that besides the singularity at $\tau_N = 0$, which also appears in other geometrical models such as circular, elliptical, and Gaussian scatter density [16], there is another singularity at $\tau_N = 1$, which is not consistent with typical experimental observations. Therefore, the ring model is not a suitable candidate for wideband channels.

A. TOA PDF of the circular ring model

In order to derive the TOA PDF of the circular ring model, $f(\tau_r \mid \tau_R^{\max})$ in (16) needs to be integrated over all possible $\tau_R^{\max} = 2R/c$, or equivalently, all possible R. For the range $0 \le \tau_r \le 2R_1/c$, all the rings affect $f(\tau_r)$ and therefore integration limits are $\tau_R^{\max} = 2R_1/c$ and $\tau_R^{\max} = 2R_2/c$. On the other hand, when $2R_1/c \le \tau_r \le 2R_2/c$, only those rings with $\tau_r \le \tau_R^{\max} \le 2R_2/c$ affect $f(\tau_r)$ and therefore the integration runs from $\tau_R^{\max} = \tau_r$ to $\tau_R^{\max} = 2R_2/c$

$$f(\tau_r) \approx \int_{2R_1/c}^{2R_2/c} f(\tau_r \mid \tau_R^{\max}) \cdot f(\tau_R^{\max}) d\tau_R^{\max}$$

$$= \begin{cases} \int_{2R_1/c}^{2R_2/c} f(\tau_r \mid \tau_R^{\max}) \cdot f(\tau_R^{\max}) d\tau_R^{\max}, & 0 \le \tau_r \le 2R_1/c, \\ \int_{\tau_r}^{2R_2/c} f(\tau_r \mid \tau_R^{\max}) \cdot f(\tau_R^{\max}) d\tau_R^{\max}, & 2R_1/c \le \tau_r \le 2R_2/c. \end{cases} \quad (18)$$

For a given $f(\tau_R^{\max})$, this integral can be calculated numerically. Note that there is only one singularity, at $\tau_N = 0$.

B. PDS of the circular ring model

The correlation function $R_T(\Delta f, \Delta t)$ for the SISO channel can be expressed as

$$R_T(\Delta f, \Delta t) = E[T(f,t)T^*(f+\Delta f, t+\Delta t)] = \Omega \rho(\Delta f, \Delta t). \quad (19)$$

using equations (4) and (14).

The PDS $P_h(\tau)$ is the inverse Fourier transform of the frequency correlation function $R_T(\Delta f, \Delta t = 0)$ [8], i.e., $P_h(\tau) = \Im_{\Delta f}^{-1}\{R_T(\Delta f, \Delta t = 0)\}$. Substitution of (19) into the definition of PDS gives equation (20) after certain manipulations and Fourier transform calculations.

$$P_h(\tau_r) \approx \begin{cases} A \int_{R_1}^{R_2} \dfrac{\exp\left[\kappa\left(\frac{c\tau_r}{R}-1\right)\cos(\mu)\right]\cosh\left[2\kappa\sqrt{\frac{c\tau_r}{2R}\left(1-\frac{c\tau_r}{2R}\right)}\sin(\mu)\right]}{\sqrt{\frac{c\tau_r}{2R}\left(1-\frac{c\tau_r}{2R}\right)}} R^{-n} f(R) dR, & 0 \le \frac{c\tau_r}{2} \le R_1, \\ A \int_{\frac{c\tau_r}{2}}^{R_2} \dfrac{\exp\left[\kappa\left(\frac{c\tau_r}{R}-1\right)\cos(\mu)\right]\cosh\left[2\kappa\sqrt{\frac{c\tau_r}{2R}\left(1-\frac{c\tau_r}{2R}\right)}\sin(\mu)\right]}{\sqrt{\frac{c\tau_r}{2R}\left(1-\frac{c\tau_r}{2R}\right)}} R^{-n} f(R) dR, & R_1 \le \frac{c\tau_r}{2} \le R_2, \end{cases} \quad (20)$$

In the above formula, A denotes a constant equal to $cD^{-n}/\left(2\pi I_0(\kappa)\right)$. Note that for the path loss exponent $n = 0$ or no path loss, all arrivals are coming with the equal strength and equation (20) differs only in the constant term from the TOA PDF, given by equations (18) and (16). In other words, under the assumption of all arrivals having equal strength, power delay spectrum is proportional to the TOA density function, i.e. $P_h(\tau_r) \propto f(\tau_r)$. The confirmation of such statement can be found in Appendix I of [17].

V. Comparison with Measured Data

To calculate the PDS and TOA PDF in (20) and (18), respectively, numerical integration should be carried out for any $f(R)$. In the sequel, we assume that scatterers are located along the radius R such that $f(R) = 2R/(R_2^2 - R_1^2)$. Note that for this kind of density function together with the special case of the uniform distribution for angle of arrival $f(\phi^U) = 1/2\pi$, i.e. $\kappa = 0$ in (11), scatterers are distributed uniformly within the circular ring, i.e. $f(x,y) = 1/[\pi(R_2^2 - R_1^2)]$, $R_1 \le \sqrt{x^2 + y^2} \le R_2$.

We have compared the PDS of the circular ring model in (20) to the empirical curve given in Fig. 6 of [15], for the high antenna position in Aarhus. Since the circular ring model produces a PDS value of infinity at $\tau_N = 0$, i.e., $\tau = \tau_{LOS}$, this point has been excluded from computing the error. The value of R_2 is determined from $R_2 = c\tau_{\max}/2 = 549\,\text{m}$, where $\tau_{\max} = 3.66\mu\text{sec}$ is the maximum relative delay [15]. The value of $\mu = \pi$ was chosen to be fixed in the calculations. Then, equation (20) has been calculated for different values of κ and R_1. The theoretical and experimental PDS curves are normalized such that the area under both is unity. For this case and based on the measured root-mean-square (RMS) delay spread of $0.4\,\mu\text{sec}$ [15], the parameters that show a reasonable fit are $\kappa = 1.3$ and $R_1 = 0.1R_2 = 54.9\,\text{m}$ (Fig. 2). The path loss exponent n was chosen to be 4, which fits typical urban environments with no LOS component. This is in accordance with channel classification made in [15]. The value of parameter $\kappa = 1.3$ is also within the range of the values reported in the Table 1 of [13].

Furthermore in Fig. 3, the TOA PDF in (18) with the same set of parameters is compared with the measured TOA PDF of a wideband outdoor channel, taken from Fig. 11 of [15]. The close agreement between the theory and empirical curve confirms the utility of the proposed wideband model.

VI. Conclusion

In this paper we have proposed the circular ring model for wideband MIMO mobile fading channels. This model provides a generic space-time-frequency correlation, suitable for simulation of frequency selective MIMO channels and efficient design of space-time coding and detection techniques over such channels. The time of arrival distribution and the power delay profile of the circular ring model are also derived and compared with published data in the literature. The close fit between the empirical data and theoretical results demonstrates the utility of circular ring model for wideband channels.

Directions for further work include comparison of AOA PDF and power azimuth spectrum (PAS) seen at the base station with the measured data given in [15]. Furthermore, a study of influence of the given cross-correlation among antennas on the performance of various types of MIMO systems might be of interest.

References

[1] J. H. Winters, "On the capacity of radio communications systems with diversity in Rayleigh fading environments," *IEEE J. Select. Areas Commun.*, vol. 5, pp. 871-878, June 1987.

[2] I. E. Telatar, "Capacity of multi-antenna Gaussian channels," *European Trans. Telecommun. Related Technol.*, vol. 10, pp. 585-595, 1999.

[3] G. J. Foschini and M. J. Gans, "On limits of wireless communications in fading environments when using multiple antennas," *Wireless Personal Commun.*, vol. 6, pp. 311-335, 1998.

[4] H. Boelcskei and A. J. Paulraj, "Space-frequency coded broadband OFDM systems" in *Proc. IEEE Wireless Commun Networking Conf.*, Chicago, IL, 2000, pp. 1-6.

[5] W. J. Choi and J. M. Cioffi, "Space-time block codes over frequency selective Rayleigh fading channels," in *Proc. IEEE Vehic. Technol. Conf.*, Amsterdam, the Netherlands, 1999, pp. 2541-2545.

[6] W. C. Jakes, Jr., *Microwave Mobile Communications*. Piscataway, NJ: IEEE Press, 1993.

[7] A. Abdi and M. Kaveh, "A space-time correlation model for multielement antenna systems in mobile fading channels", *IEEE J. Select. Areas Commun.*, vol. 20, pp. 550 -560, 2002.

[8] P. A. Bello, "Characterization of randomly time-variant linear channels," *IEEE Trans. Commun. Sys.*, vol. 11, pp. 360-393, 1963.

[9] B. H. Fleury, "First- and second-order characterization of direction dispersion and space selectivity in the radio channel," *IEEE Trans. Inform. Theory*, vol. 46, pp. 2027–2044, 2000.

[10] G. L. Stuber, *Principles of Mobile Communication*. Boston, MA: Kluwer, 1996.

[11] T. A. Chen, M. P. Fitz, W. Y. Kuo, M. D. Zoltowski, and J. H. Grimm, "A space-time model for frequency nonselective Rayleigh fading channels with applications to space-time modems," *IEEE J. Select. Areas Commun.*, vol. 18, pp. 1175–1190, 2000.

[12] W. C. Y. Lee, "Effects on correlation between two mobile radio base station antennas," *IEEE Trans. Commun.*, vol. 21, pp. 1214–1224, 1973.

[13] A. Abdi, J. A. Barger, and M. Kaveh, "A parametric model for the distribution of the angle of arrival and the associated correlation function and power spectrum at the mobile station," *IEEE Trans. Veh. Technol.*, vol. 51, pp. 425-434, 2002.

[14] I. S. Gradshteyn and I. M. Ryzhik, *Table of Integrals, Series, and Products*, 5th ed, A. Jeffrey, Ed. San Diego, CA: Academic, 1994.

[15] K. I. Pedersen, P. E. Mogensen, and B. H. Fleury, "A stochastic model of the temporal and azimuthal dispersion seen at the base station in outdoor propagation environments," *IEEE Trans. Vehic. Technol.*, vol. 49, pp. 437–447, 2000.

[16] R. Janaswamy, "Angle and time of arrival statistics for the Gaussian scatter density model," *IEEE Trans. Wireless Commun.*, vol. 1, pp. 488–497, 2002.

[17] P. Hoeher, "A statistical discrete-time model for the WSSUS multipath channel," *IEEE Trans. Vehic. Technol.*, vol. 41, pp. 461–468, 1992.

[18] J. Fuhl, A. F. Molisch and E. Bonek, "Unified channel model for mobile radio systems with smart antennas," *IEE Proc. Radar, Sonar and Navigation*, vol. 145, pp. 32-41, 1998.

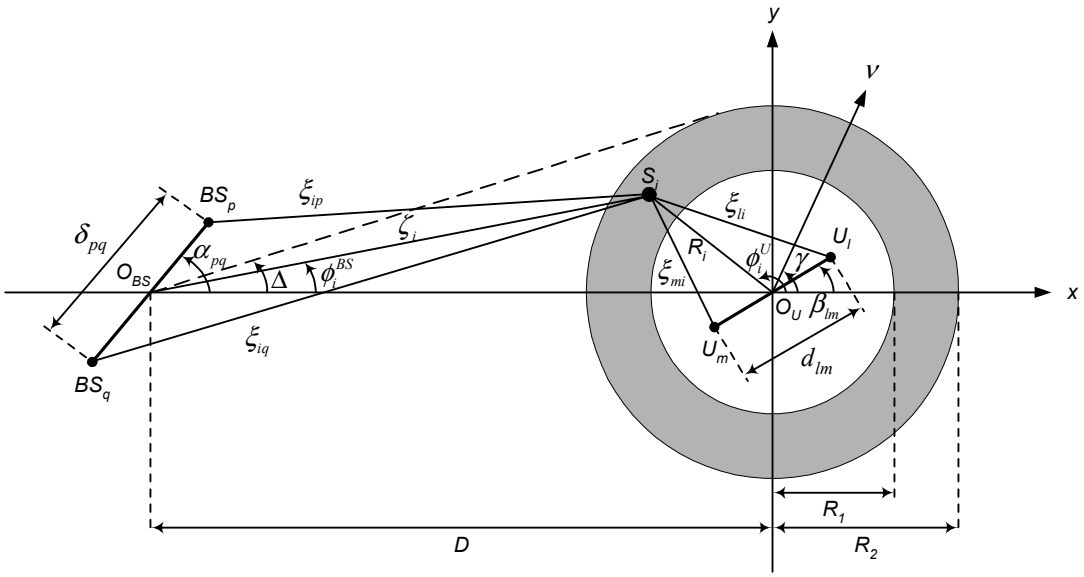

Fig. 1. Geometrical configuration of a 2×2 circular ring channel with local scatterers around the mobile user (two-element arrays at the BS and the user).

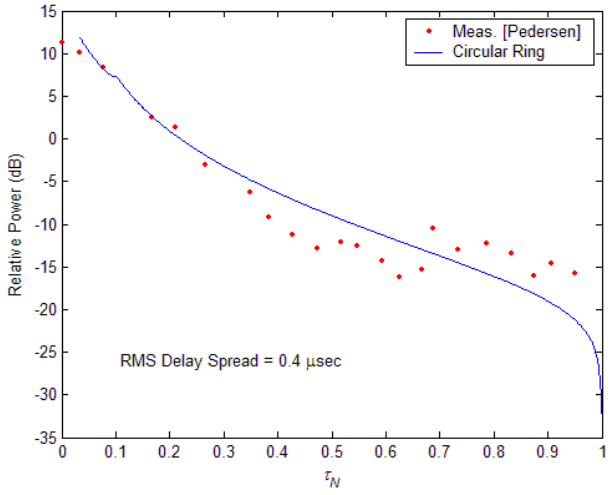

Fig. 2. Comparison of the power delay spectrum of the circular ring model with measurements.

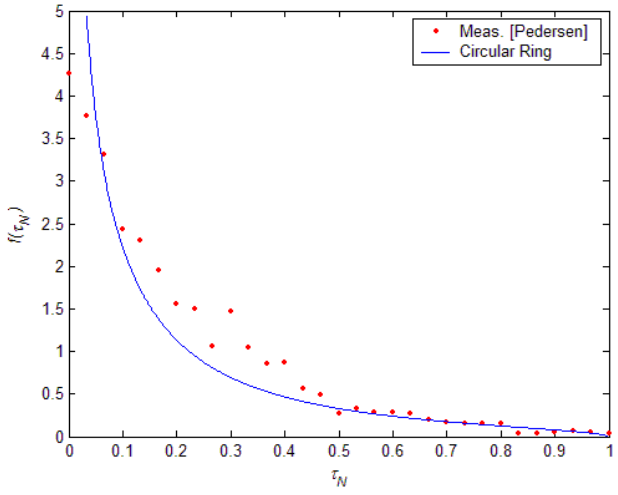

Fig. 3. Comparison of the TOA PDF of the circular ring model with measurements.